Extratropical cyclones over the North Atlantic and Western Europe during the Last Glacial Maximum and implications for proxy interpretation

Joaquim G. Pinto[1] and Patrick Ludwig[1]

[1]Institute of Meteorology and Climate Research, Karlsruhe Institute of Technology, 76131 Karlsruhe, Germany

Correspondence to: Joaquim G. Pinto (joaquim.pinto@kit.edu)

Abstract. Extratropical cyclones are a dominant feature of the mid-latitudes, as their passage is associated with strong winds, precipitation, and temperature changes. The statistics and characteristics of extratropical cyclones over the North Atlantic region exhibit some fundamental differences between Pre-Industrial (PI) and Last Glacial Maximum (LGM) climate conditions. Here, the *statistics* are analysed based on results of a tracking algorithm applied to global PI and LGM climate simulations. During the LGM, both the number and the intensity of detected cyclones was higher compared to PI. In particular, increased cyclone track activity is detected close to the Laurentide ice sheet and over central Europe. To determine changes in cyclone *characteristics*, the top 30 extreme storm events for PI and LGM have been simulated with a regional climate model and high resolution (12.5 km grid spacing) over the eastern North Atlantic and Western Europe. Results show that LGM extreme cyclones were characterised by weaker precipitation, enhanced frontal temperature gradients, and stronger wind speeds than PI analogues. These results are in line with the view of a colder and drier Europe, characterised by little vegetation and affected by frequent dust storms, leading to reallocation and build-up of thick loess deposits in Europe.

1. Introduction

The day-to-day weather conditions in the mid-latitudes are strongly affected by the passage of extratropical cyclones, which are typically associated with precipitation, strong winds, and changes in temperature and cloudiness. Cyclones also play a major role in the water cycle and the redistribution of momentum and energy in the climate system (Hoskins and Valdez, 1990: Chang et al., 2002). The assessment of cyclone activity, notably to analyse their paths, characteristics and impacts are thus key to determine both the day-to-day weather conditions, the regional mean climate and its variability on multiple time-scales. In fact, there is a wide range of literature analysing case studies of extreme cyclones (e.g., Wernli et al., 2002; Ludwig et al., 2015), the mean cyclone activity in the mid-latitudes in the recent past (e.g., Hoskins and Hodges, 2002; Ulbrich et al., 2009) and possible changes under future climate conditions (e.g., Bengtsson et al., 2009; Ulbrich et al., 2009). On the other hand, studies analysing the structural characteristics of extratropical storms from a climatological perspective are less frequent (e.g. Catto et al., 2010; Rudeva and Gulev, 2011; Dacre et al., 2012; Hewson and Neu, 2015; Sinclair et al., 2019). While some

general concepts are available on how warmer climate conditions will affect the intensity and structure of cyclones, there are still several open questions, particularly regarding how dominant the increased latent heating may become compared to other physical processes like low-level and upper-level baroclinicity (see Catto et al., 2019; their Figure 2).

The availability of studies addressing the characteristics of cyclone activity outside of the period extending from the mid-19th Century to the end of the 21st-Century decreases sharply. Raible et al (2018) analysed variations of cyclone statistics in a very long simulation with a fully coupled earth system model from 850 to 2100 CE. While they identified variations on multiple time-scales, they found no evidence for an external forcing imprint before 1850. Moreover, Pfahl et al. (2015) analysed cyclone activity in idealised aquaplanet simulations covering a wide range of possible climate conditions (from 270K to 316K global mean temperatures). While the structure of the majority of the cyclones reveals only small changes on average, larger differences were identified for intense cyclones. For example, cross-front temperature differences are expected to be higher (lower) for considerably colder (warmer) climates (Pfahl et al., 2015, their Figure 10), whereas the associated precipitation is expected to decrease (increase; their Figure 12) due to the strong limiting effect of temperature on the atmospheric moisture content.

One important issue preventing non-recent or non-21st century cyclone analysis is the availability of climate model output with sufficient spatial and temporal resolution to enable identification, tracking and characterisation of such cyclones. For example, model data from the PMIP3 project (Braconnot et al., 2012) are only archived 6-hourly for short (30 years) time slices, and typically at a low resolution (approximately 200-300 km). Most pre-20th Century studies consider aggregated measures of cyclone (or synoptic) activity (e.g., Kageyama et al., 1999; Laine et al., 2009; Hofer et al., 2012; Ludwig et al, 2016), thus not enabling a detailed comparison to regional temperature and precipitation variability. One period of particular interest is the Last Glacial Maximum (LGM; Clark et al., 2009), when the European climate was characterised by colder and mostly drier conditions (Bartlein et al., 2011; Annan and Hargreaves, 2013; Újvári et al., 2017; Cleator et al., 2019). Large parts of Northern Europe were covered by permanent ice sheets and surrounded by polar-desert conditions (Ray and Adams, 2001). Western, Central and Eastern Europe were largely characterised by open shrublands and grasslands (steppe-tundra), while in Southern Europe steppe with embedded forest (forest steppe) dominated (Ray and Adams, 2001). Under these conditions, dust storms triggered by strong winds must have been common in Europe, as documented by the major loess deposits found primarily around 50°N over Western and Central Europe and over large parts of Eastern Europe (Antoine et al., 2009; 2013; Sima et al., 2013; Újvári et al., 2017).

Under the influence of the continental ice sheets and extended sea ice, the PMIP3 GCMs show stronger meridional temperature gradients, leading to a southward displaced, more intense and less variable North Atlantic jet than under current climate conditions (Löfverström et al, 2014; 2016; Merz et al., 2015; Wang et al. 2018). These differences have been related e.g., to more dominant cyclonic Rossby wave breaking near Greenland (Riviére et al., 2010), stationary wave packets trapped in the mid-latitude wave guide (Löfverström, 2020) and to enhanced meridional eddy momentum flux convergence over the North Atlantic (Wang et al., 2018). In line with a southward displaced and stronger jet stream, several studies show a more intense

and southward shifted North Atlantic storm track compared to today's climate (e.g., Hofer et al., 2012; Luetscher et al., 2015; Ludwig et al., 2016). However, other studies display reduced storm track activity over the North Atlantic in spite of the enhanced baroclinicity (e.g. Donohoe and Battisti, 2009; Riviére et al., 2010; Löfverström et al., 2016). Riviére et al. (2018) discusses a reduced baroclinic conversion as a possible reason for this apparent discrepancy, arguing that the eddy heat fluxes are less well aligned with the mean temperature gradient for LGM than for PI. Other arguments for the reduced storminess include model resolution, parameterizations and boundary conditions (e.g. Donohoe and Battisti, 2009; Riviére et al., 2018). Thus, the intensity differences between LGM and PI North Atlantic storm track activity may be model dependent.

The PMIP3 models show indications that while Europe was largely drier than today, this is not the case for some regions, notably for Iberia (e.g., Hofer et al., 2012; Beghin et al., 2016, Ludwig et al., 2016). However, wetter conditions over Iberia are not in line with (most of) the proxy data, which themselves are often associated with considerable uncertainties (e.g., Bartlein et al., 2011; Moreno et al., 2014, Cleator et al., 2019). Nevertheless, the substantial misrepresentation of the regional climate for the LGM in PMIP3 models compared to proxies is regarded as a general issue (Harrison et al., 2015). In some cases, such caveats can be partially traced back to shortcomings of the GCMs and/or their boundary conditions. For example, Ludwig et al (2017) implemented more realistic boundary conditions in terms of the North Atlantic SSTs, land use types and vegetation cover in a regional climate model (RCM) to simulate the regional climate under LGM conditions. Their results in terms of LGM temperature, precipitation and the permafrost margin are in better agreement with the proxies than without the implemented boundary conditions. Still, further studies are needed, notably at the regional scale (e.g. Ludwig et al., 2018), in order to further our confidence in the modelling capabilities and our understanding of the paleoclimate conditions for Europe in key periods like the LGM (Harrison et al., 2015; 2016; Ludwig et al., 2019).

The present work aims to advance our understanding of the LGM climate over the North Atlantic and Europe through a more detailed analysis of the cyclonic activity and its associated impacts, notably in terms of precipitation, temperature and wind speed. The LGM cyclones are first identified and tracked on a simulation with the coupled MPI-ESM-P model, for which data with high temporal resolution was archived. Secondly, a sub-sample of extreme cyclones is downscaled with a RCM to analyse possible changes in LGM cyclone characteristics compared to their modern counterparts at high spatial and temporal resolution. The identified characteristics of LGM extreme cyclones are discussed in terms of the available proxies for LGM Climate across Western Europe. Additionally to the precipitation and temperature, the importance of the dominant land cover conditions and the frequent occurrence of dust storms is evaluated. The final section presents the summary and main conclusions.

2. Data and Methods

The starting point of our analysis is data from the third phase of the Paleoclimate Modeling Intercomparison Project (PMIP3) (Braconnot et al., 2012) (http://pmip3.lsce.ipsl.fr/). The simulations were performed according to the PMIP3 21 ka

experimental design, which includes the lower sea level and blended ice sheet data (Peltier et al., 2015, Lambeck and Chappell, 2001; Lambeck et al., 2002; Tarasov and Peltier, 2002, 2003), orbital parameters and lower greenhouse gas concentrations (see Table 1). From the PMIP3 GCMs, we have selected the MPI-ESM-P (Stevens et al., 2013; Jungclaus et al., 2013) constant forcing simulations, for which two 30-year time slices with six hourly output data are available for Pre-Industrial (PI) and LGM conditions. This choice was motivated by the availability of six hourly 3-D model level data needed for running the RCM. Ludwig et al. (2016) recently analysed a small ensemble of PMIP3 models in terms of large-scale circulation for Europe, jet stream synoptic activity, precipitation and temperature for the LGM. While the MPI-ESM-P model has a slightly different jet structure to some of the other PMIP3 models (cf. Ludwig et al., 2016; their Figure 2), which also impacts for example the storm track and precipitation (their Figures 4, 6), its main characteristics are generally close to the ensemble average.

Individual extratropical cyclones over the North Atlantic and Europe are identified and tracked based on six hourly mean sea level pressure data with a widely used automatic tracking algorithm (Murray and Simmonds, 1991; Pinto et al. 2005). The resulting cyclone statistics provide information on the lifetime of each identified cyclone, thus enabling the computation of mean cyclone statistics like track density, mean maximum intensity, cyclogenesis, cyclolysis, propagation speed and deepening rates. Cyclone statistics obtained with this method compare well with other methodologies (e.g., Neu et al., 2013; Hewson and Neu, 2015). Following Pinto et al. (2009), cyclones are selected based on the following conditions: (a) cyclone lifetime of at least 24 h hours, (b) a minimum core MSLP value below 1000 hPa (3) a maximum vorticity (approximated by the Laplacian of MSLP) value above 0.6 hPa deg. lat.$^{-2}$, and (d) a maximum deepening rate of 0.3 hPa deg. lat.$^{-2}$s^{-1} is achieved at least once during their lifetime. The method is here applied to the MPI-ESM-P data for the extended (ONDJFM) winter season. In order to analyse the characteristics of the most extreme cyclones affecting Europe in more detail, the most intense 30 cyclones (TOP 30) for the PI and LGM periods are selected based on their peak intensity in terms of vorticity and their passage within a pre-defined box over the eastern North Atlantic (Figure 1, dashed box). The selection of the box enables the creation of a cyclone ensemble that impacts Western Europe and permits a comparison with terrestrial proxy data e.g. for precipitation and dust.

The Weather Research and Forecast (WRF) model (Skamarok et al., 2008) is used in its version 3.9.1.1 to simulate the TOP 30 cyclones (from PI and LGM) with a grid spacing of 12.5 km (including 35 vertical layers up to 30 hPa). To achieve a grid spacing of 12.5 km, a 2-step nesting approach is necessary. Cyclones were initially simulated on a 50 km grid forced by MPI-ESM-P data as initial and boundary conditions with an update frequency of six hours. The final 12.5 km grid spacing is achieved by a second nesting step within the WRF model. An overview of the parameterization choices is given in Table 2. For the calculation of wind gusts, a gust parameterization based on 10 m wind speed and friction velocity (Schulz and Heise, 2003; Schulz, 2008) has been implemented into the WRF model. This gust parameterization shows an overall good agreement with observed wind gusts, particularly over flat terrain (Born et al. 2012). For the WRF simulations, global PI and LGM boundary conditions were adapted considering specifications of the PMIP3 protocol (Braconnot et al., 2012, see also Ludwig

et al. 2017). These changes encompass orbital parameters, trace gases (see Table 1), the consideration of ice sheets (extent and height), an associated lowering of the sea level and adaption of land use cover (CLIMAP Project Members, 1984).

The TOP 30 cyclone tracks simulated by WRF were identified manually based on relative vorticity field at 850 hPa. For comparison of the PI and LGM cyclone characteristics, and following the methodology from Catto et al. (2010; their Figure 3), each track was rotated so that the cyclones were each moving in west-east direction, enabling the generation of composites for different atmospheric variables (cf. also Dacre et al., 2012). Composites have been created for peak intensity (0) and 6, 12,18 and 24 hours before peak intensity, and 6 and 12 hours afterwards. For brevity, we will primarily discuss the time frames i) 12 hours before peak intensity and ii) peak intensity. The variables analysed from the 12.5 km WRF simulations include mean sea level pressure, precipitation, column integrated water vapour, equivalent-potential temperature 850 hPa, 925 hPa winds, near-surface wind gusts.

3. Northern Hemisphere Cyclone Statistics for PI and LGM conditions

In this section, we analyse the general characteristics of cyclones over the North Atlantic and Europe under LGM conditions and compare them to PI climate conditions. Figure 2 shows the cyclone track density for the extended winter for PI and LGM climate conditions. In spite of the lower spatial resolution of MPI-ESM-P, the cyclone track density for the PI is close to cyclone statistics obtained with Reanalysis datasets, with slight southerly shift of cyclonic activity (see Figure S1 for comparison with NCEP reanalysis data (Kalnay et al, 1996)), and CMIP GCMs for recent climate conditions (cp. Pinto et al., 2007; their Figure 1). Still, some regional shortcomings are identified, notably the limited cyclone activity over the Mediterranean basin. The North Atlantic storm track shows a clear tilt towards Northern Europe and the Arctic Ocean for PI, and its location and orientation are closely related with the eddy-driven jet stream (black contours in Fig. 2a) and the associated upper-air baroclinicity (Hoskins and Valdes, 1990; Pinto et al., 2009). A comparison of the jet stream between MPI-ESM-P PI and NCEP Reanalysis data shows a slight tilt towards Europe by the MPI model (Fig. S2), in line with the enhanced (reduced) southward (northward) cyclone activity (Fig. S1)

The North Atlantic storm track looks quite different under LGM conditions relative to PI: the cyclone track density is higher over the North Atlantic and more constrained to the ice edge (Fig. 2b, Fig. S1). Close to Europe, a bifurcation is found, and cyclones are either deflected northward along the border of the Scandinavian ice sheet or south-eastward towards Central Europe and the Mediterranean (Fig. 2c). In accordance, the eddy-driven jet is stronger under LGM conditions in the MPI-ESM-P (Fig. S2), thus establishing more favourable conditions for the occurrence of intense storms affecting Western and Central Europe. For the North Atlantic (70°W – 0°, 35°N – 70°N), the total number of cyclones for the analysed 30-year period is about 26% larger for LGM than for PI conditions (12071 vs. 9541 individual cyclone counts in 30 years, corresponding to roughly 2.2 cyclones/day vs 1.8 cyclones/day).

Other properties of cyclone activity are depicted in Figure 3 for LGM in terms of absolute values (left column) and their differences to PI (right column). Cyclogenesis is dominant along the North American east coast for the LGM (Fig. 3a), and much stronger than in PI (Fig. 3b), which is in line with a much stronger upper level jet stream during glacial conditions. Moreover, the rate of cyclogenesis increased south of Greenland and over Western and Central Europe. On the other hand, there is more cyclolysis along the borders of the Greenland and Scandinavian ice sheet (Fig. 3c) relative to the PI conditions (Fig. 3d). Mean maximum cyclone intensity is typically attained in a region extending from Newfoundland to Iceland and the British Isles, with a secondary maximum over Eastern Europe (Fig. 3e). Compared to the PI cyclones, the LGM cyclones have stronger intensities, particularly in an area extending from the south of Greenland to the British Isles, and over most of continental Europe. On the other hand, cyclone intensity close to the North American East coast is considerably lower (Fig. 3f). Deepening rates are stronger for LGM cyclones over the central north Atlantic, as well as their filling rates close to the ice edge / ice sheets (Fig. 3g,h). These results point towards different typical development of LGM cyclones compared to their PI counterparts, which occurs either more zonally at lower latitudes towards Central Europe or further downstream closer to the ice edge towards the Arctic.

Figure 4 displays the relative frequency distribution of the cyclone intensity over the North Atlantic area (70°W – 0°, 35°N – 70°N), revealing that LGM cyclones are on average more intense (mean (median): 1.58 (1.41) hPa deg. lat.$^{-2}$s^{-1}) than their PI counterparts (mean (median): 1.43 (1.28) hPa deg. lat.$^{-2}$s^{-1}). In particular, the number of cyclones exceeding 3 hPa deg. lat.$^{-2}$s^{-1} is twice as large for LGM than for PI. In fact, a small number (18) of LGM cyclones attain intensities exceeding the range identified for PI cyclones. The statistics for the region close to Europe (box) are similar (not shown). All these results document a shift towards stronger intensities for LGM cyclones, both in terms of average numbers and extreme values.

4. Characteristics of Extreme Cyclones over the Eastern North Atlantic

To analyse the characteristics of cyclones for the LGM, a subset of 30 extreme cyclones passing over the Eastern North Atlantic is selected for both the PI and LGM periods based on the highest values for vorticity (Laplacian of MSLP) within the selected box. The trajectories of the selected MPI-ESM cyclones are depicted in Figure 5 and key information are given in Table 3. Two important facts are clearly identifiable: LGM extreme cyclone trajectories are more zonally orientated and constrained to a narrower corridor (particularly until 15°W) than their PI counterparts, and they achieve higher vorticity (mean Laplacian of MSLP for LGM: 2.80; PI: 2.52) values during lifetime (Tab. 3).

For each of these cyclones, WRF simulations down to 12.5 km grid-spacing are performed along the most intense segment of their lifetimes, thus gaining 3D data to analyse the cyclones e.g. in terms of the evolution of their structure, air masses, winds and precipitation. Care was taken that storms agree between the original MPI-ESM-P data and WRF cyclone tracks. Generally, the obtained tracks based on the WRF simulations reveal lower core pressures and higher vorticity than their low resolutions counterparts do. Figure 6 shows a comparison between high and low resolution data for a selected cyclone. The considered

cyclone tracks (MPI-ESM LGM cyclone #24) show a good superimposition for MPI-ESM, WRF 50 km and WRF 12.5 km and a good agreement of the position of maximum intensity with a slightly further south-eastward location for WRF 50 km (Fig. 6a). While the time series, centred at peak intensity, for the development of core pressure show a similar strong pressure drop for all resolutions, the relative vorticity exhibits much stronger values for the high resolution simulation (WRF 12.5 km) in comparison with the coarser realisations. Note that the WRF simulations do not cover the whole trajectory of the cyclones, and thus the time series are shorter. Figure 6c and 6d depict the corresponding precipitation patterns at peak intensity, in this case revealing more small scale structures and higher precipitation values for the 12.5 km WRF simulation.

Based on the top 30 cyclones for PI and LGM and using the composite methodology described in section 2, average cyclone characteristics are investigated for the intensification phase, focussing on the time frames (i) 12 hours before peak intensity and (ii) peak intensity. Figure 7 displays the MSLP fields for PI and LGM for peak intensity; the corresponding panels for 12 hours before peak intensity can be found in Fig. S3. The anomalies compared to the mean MSLP are displayed in colours, in order to analyse MSLP gradients (Fig. 7 a,b; S3 a,b). The core MSLP of the LGM has higher values compared to PI (LGM: 982.7 hPa, PI: 975.2 hPa). This can be explained by the lower sea levels (~120m) for LGM, causing a difference of global mean sea level pressure of about ~13 hPa (PI: 1010 hPa, LGM: 1023 hPa). Taking this into account, the LGM cyclones reach deeper MSLP values compared to the global average MSLP, being consistent with the stronger deepening rates for LGM cyclones identified by the tracking algorithm (Fig.3 g,h). Additionally, the closer isobars south of the cyclone core indicate stronger pressure gradients for the LGM cyclones, which is supported by the LGM – PI differences (Fig. 7c). This is particularly the case on the expected location of the frontal areas. Fig. 7 (d,e) and Fig. S3 (d,e) displays the anomalies of potential temperature at 850 hPa for LGM relative to PI. Results show that the cross-frontal gradients are particularly intense across the warm front and that the whole development is displaced forward in the cyclone for LGM conditions, indicating a faster occlusion (Fig. 7 f). On the other hand, the total water content is much higher under PI conditions, primarily due to the effect of the higher environmental temperatures (Fig. 7 g,h; Fig. S3 g,h) with differences in the warm sector reaching up to 10 mm and 6-8 mm close to the cyclone core at peak intensity (Fig. 7i).

The strong difference in available water content again leads to a large difference in terms of accumulated precipitation, which is clearly larger for the PI composites (Fig. 8 a,b; Fig. S4 a,b). While some of the smaller deviations can be potentially attributed to slightly different developments, the total precipitation is considerably lower for the LGM extreme cyclones (up to 1.7 mm h^{-1}) particularly in the area of peak precipitation close to the cyclone centre (Fig. 8c). On the other hand, wind speed at 925 hPa is much higher for LGM cyclones (Fig. 8 d,e; Fig. S4 d,e), where wind speeds over large areas south of the cyclone exceed their PI counterparts by 10-12 ms^{-1}, particularly for 12 hours before peak intensity (Fig. 8 f; Fig. S4 f). Strong differences are also revealed for near-surface wind gusts (Fig. 8 g-i; Fig. S4 g-i). In this case, the wind gusts are particularly enhanced along the expected location of the cold front at peak intensity, with deviations exceeding 5 ms^{-1}. The above described patterns remain true for the cyclone characteristics 12 hours after peak intensity (Figs S5, S6). For example, stronger wind gusts remain dominant in the area south of the cyclone core (Fig. S4i).

In summary, LGM cyclones display steeper MSLP gradients (in agreement with higher intensity in terms of circulation), larger temperature gradients between the air masses, weaker precipitation and stronger wind gusts than their PI counterparts do (see also summary for wind and precipitation in Table S1).

5. Discussion with available proxy-based climate reconstructions

The above analysis shows that extreme cyclones under LGM conditions were typically more intense than PI extreme cyclones. Likewise, they were associated with larger frontal temperature gradients, stronger winds and reduced precipitation. In this section, we analyse in how far these cyclone characteristics can help to explain the climate conditions in Western and Central Europe at the LGM and the frequent occurrence of dust storms in that area.

According to the available proxy records, Western and Central Europe were colder and largely drier under LGM conditions (Bartlein et al., 2011; Annan and Hargreaves, 2013; Cleator et al., 2019), and was to a large extent covered by open shrublands and grasslands (Ray and Adams, 2001). The colder and generally drier conditions are reproduced by the PMIP3 GCMs, but considerable differences in detail have been identified compared to proxy-based climate reconstructions (Beghin et al., 2016; Ludwig et al., 2016; Cleator et al., 2019). These can be both attributed to shortcomings of the GCMs and/or uncertainties in the reconstructions, which are often not well constrained (Bartlein et al., 2011; Ludwig et al., 2019; Cleator et al., 2019). For example, most PMIP3 GCMs show enhanced precipitation over the Iberian Peninsula compared to PI climate (Beghin et al., 2016; Ludwig et al., 2016), which disagrees with the proxy data (e.g. Bartlein et al., 2011). Later, Ludwig et al (2017, 2018) show that the wet bias over Iberia and Western Europe can strongly be reduced by considering more realistic boundary conditions (particularly in terms of sea surface temperatures, land use and vegetation cover) in high-resolution RCM simulations.

The present results enable a more detailed evaluation of the above hypotheses and interpretations. Under current climate conditions, precipitation in the mid-latitudes is largely associated with the passage of extratropical cyclones, where extreme cyclones have a comparatively larger contribution to total/extreme precipitation (Pfahl and Wernli, 2012; Hawcroft et al. 2012). Hawcroft et al. (2016) have provided evidence that GCMs typically have shortcomings in representing the precipitation associated with mid-latitude cyclones. It is reasonable to assume that those shortcomings may be exacerbated at lower resolutions, e.g. those typical of the PMIP3 models. An idealised study by Pfahl et al. (2015) has shown that precipitation increases (decreases) disproportionately in considerably warmer (colder) climate conditions. With the help of the high resolution WRF simulations, we could provide evidence that extreme cyclones under LGM conditions indeed induce considerably less precipitation than their PI counterparts (~22% within a 10° radius around the cyclone centre). Even though lower cyclone-related precipitation may be partially compensated by enhanced moisture advection embedded in the (stronger) westerly large-scale flow, particularly for areas where orographic precipitation dominates (e.g. upward slopes of mountain ranges / glaciers), it is consistent with the hypothesis of a drier Western and Central Europe. The view of a drier Europe is also

consistent with the dominant land cover types estimated from proxy data (Ray and Adams, 2001) or a statistical reconstruction based on temperature and precipitation (Shao et al., 2018), namely polar desert close to the glaciers, forest steppe over Southern Europe and steppe in-between. The fact that we have selected an area close to the Iberian Peninsula for cyclone selection leads to the strong assumption that largely drier conditions must also have been found for Southwestern Europe, in agreement with the proxies (e.g. Bartlein et al., 2011, Moreno et al., 2014).

Mineral dust plays an important role in our climate system (Shao et al., 2011). Dust emissions are typically initiated by the wind stress on land surfaces with little to no vegetation cover and easily erodible soils (e.g., Prospero et al., 2002). Such areas were very common in Europe under LGM conditions (e.g., Ray and Adams, 2001, Ugan and Byers, 2007), when the global dust cycle is estimated to have been stronger than at present (Maher et al., 2010). A large number of loess deposits over Western and Central Europe (particularly around 50°N; Antoine et al., 2009) indicate that dust storms were a common feature of the European climate. In particular, Antoine et al. (2009) identified cyclic variations in loess deposition between 34-17 ka on several sites in France, Germany and Belgium, with particularly high sedimentation rates, and attributed these to numerous and intense dust storms in periods with stronger large-scale flow and reduced precipitation. Furthermore, the high accumulation rates of loess in the middle and lower Danube basin indicate cold, dry and windy conditions during the LGM in south-eastern Europe (Fitzsimmons et al, 2012), consistent with increased storm activity over Central Europe (Fig. 2c). These and other findings document a more intense (global) dust cycle for LGM conditions (e.g. Albani et al., 2016; Újvári et al., 2017; Albani and Mahowald, 2019). The occurrence of dust storms over Western and Central Europe has been conceptually associated with the passage of intense extratropical cyclones penetrating deep into the continent (Antoine et al., 2009; their Figure 12). Following on previous studies (e.g. Laine et al., 2009; Hofer et al. 2012; Ludwig et al., 2016), the present results provide evidence for the first time that individual LGM cyclones would be indeed capable of triggering such dust events: their frequent tracks over Western/Central Europe and strong wind could easily trigger dust emission and transport over short (for coarse grain) and large (for fine grain material) distances (cp. Shao et al. 2011). As moisture acts to make surface dust particles more cohesive (e.g., Ishizuka et al., 2008), the reduced cyclone precipitation and higher wind speeds in LGM cyclones would have actually been more conducive to generating dust storms. In addition to the role of the westerlies and embedded cyclones into generating dust storms in Europe, there is evidence that situations with persistent easterlies associated with anticyclonic flow triggered by a strong anticyclone over the Scandinavian ice sheet may have also played a significant role for loess deposition not only over Eastern Europe but also over Central Europe (Újvári et al., 2017; Schaffernicht et al., 2019).

6. Summary and Conclusions

The statistics and characteristics of extratropical cyclones over the North Atlantic and Western Europe were analysed for time-slice experiments for PI and LGM conditions. First, the statistics of the climatologies of PI and LGM cyclones are analysed and compared based on global MPI-ESM-P simulations. Second, the characteristics of extreme LGM cyclones over the Eastern

North Atlantic were analysed in detail based on high-resolution simulations (12.5 km grid-spacing) with the RCM WRF and compared to their PI counterparts. The results were discussed with available proxy reconstructions of climate parameters and vegetation types. The main conclusions are as follows:

- The North Atlantic storm track was more intense under LGM conditions, featuring more frequent and intense synoptic systems than under PI conditions. One of the downstream branches brought more often extreme cyclones towards Western and Central Europe and the Mediterranean area.
- LGM cyclones were more intense due to stronger baroclinicity with less influence from diabatic processes (lower rainfall and lower water vapour content). In particular, LGM cyclones benefit from a stronger and extended jet stream. The development was typically faster, with deepening rates and peak intensities exceeding those from PI cyclones.
- LGM extreme cyclones were characterised by lower precipitation, enhanced frontal temperature gradients, and stronger mean wind speeds and wind gusts than PI analogues.
- These characteristics are in line with the view of a colder and drier Europe, characterised by steppe/tundra land types and affected by frequent dust storms, leading to reallocation and build-up of thick loess deposits.

Given that this study is based on a single GCM, a single tracking method and a single RCM, it should be regarded as a preliminary analysis as the uncertainties of the jet stream position and storm track activity (e.g., Merz et al, 2013, Riviere et al., 2018) may be considerable among different GCMs. Still, the identified differences between PI and LGM (extreme) cyclones are unequivocal, are consistent with idealised studies, demonstrate the potential of the approach and may become instrumental to facilitate a better interpretation of LGM proxy data. In particular, this study provides new understanding of the relationship between the large scale mean cyclone activity and short term variability on the regional scale and thus may help to reduce numerical interpretative uncertainties (Harrison et al. 2016).

Even though the added value of RCMs in paleoclimate applications is still controversially discussed (Armstrong et al., 2019), there is a general call for improvements towards a new generation of reliable regional projections (e.g., Harrison et al., 2015; Kageyama et al., 2018). The present and other studies (see Ludwig et al., 2019 for a review) provide clear arguments for the extended use of RCMs in the scope of paleoclimate studies, as they can play an important role towards a meaningful joint interpretation of proxies and climate model data. The upcoming new paleoclimate simulations within CMIP6/PMIP4 (Kageyama et al., 2017, 2018), as well as new proxy-based reconstructions of climates (Cleator et al. 2019), will provide novel possibilities to expand our understanding of past climates and to reduce uncertainties on both the numerical and reconstruction branches.

Data availability: WRF-Data presented in the paper can be accessed by contacting the authors. The data will be archived at the DKRZ (German Climate Computing Centre). PMIP3 boundary conditions can be obtained at https://pmip3.lsce.ipsl.fr/

(last access: 12 November 2019). Vegetation cover and Landuse data from CLIMAP can be obtained at https://iridl.ldeo.columbia.edu/SOURCES/.CLIMAP/.LGM/ (last access: 12 November 2019).

Author contributions: Both authors contributed equally to this work. JGP and PL designed the study and the experiments. PL developed the paleo-specific model adjustments, performed the simulations and prepared the figures. JGP wrote the first draft of the manuscript. JGP and PL contributed with revisions.

Competing interests: The authors declare that they have no conflict of interest.

Acknowledgements: We thank the German Climate Computing Centre (DKRZ, Hamburg) for providing the MPI-ESM-P data and computing resources within DKRZ Project 965 "Our Way to Europe – Palaeoclimate and Palaeoenvironmental reconstructions". JGP thanks the AXA Research Fund for support, and both authors thank REKLIM (Helmholtz Climate Initiative regional climate change) for partial funding. Thanks to Alexander Reinbold for his contribution to a preliminary analysis, and Sven Ulbrich for help with the cyclone statistics. The authors also thank the PALEOLINK project by the PAGES 2kNetwork coordinators. We acknowledge support by Deutsche Forschungsgemeinschaft (DFG) and Open Access Publishing Fund of Karlsruhe Institute of Technology. We thank two anonymous reviewers and M. Löfverström for the detailed and helpful comments.

References

Albani, S., Mahowald, N.M., Murphy, L.N., Raiswell, R., Moore, J.K., Anderson, R. F., McGee, D., Bradtmiller, L.I., Delmonte, B., Hesse, P. P., et al.: Paleodust variability since the Last Glacial Maximum and implications for iron inputs to the ocean, Geophys. Res. Lett., 43, 3944– 3954, doi:10.1002/2016GL067911, 2016.

Albani, S. and Mahowald, N.M.: Paleodust Insights into Dust Impacts on Climate. J. Climate, 32, 7897–7913, doi:10.1175/JCLI-D-18-0742.1, 2019.

Annan, J. D., and Hargreaves, J. C.: A new global reconstruction of temperature changes at the Last Glacial Maximum, Clim. Past, 9, 367-376, doi:10.5194/cp-9-367-2013, 2013.

Antoine, P., Rousseau, D.-D., Moine, O., Kunesch, S., Hatté, C., Lang, A., Tissoux, H., and Zöller, L.: Rapid and cyclic aeolian deposition during the Last Glacial in European loess: a high-resolution record from Nussloch, Germany, Quat. Sci. Rev., 28, 2955–2973, doi:10.1016/j.quascirev.2009.08.001, 2009.

Antoine, P., Rousseau, D. D., Degeai, J.-P., Moine, O., Lagroix, F., Kreutzer, S., Fuchs, M., Hatté, C., Gauthier, C., Svoboda, J., and Lisa, L.: High-resolution record of the environmental response to climatic variations during the Last Interglacial-

Glacial cycle in Central Europe: the loess-paleosol sequence of Dolni Vestonice (Cezch Republic), Quaternary Sci. Rev., 67, 17–38, doi:10.1016/j.quascirev.2013.01.014, 2013.

Armstrong, E., Hopcroft, P. O., and Valdes, P.: Reassessing the value of regional climate modelling using palaeoclimate simulations. Geophysical Research Letters, 46, doi:10.1029/2019GL085127, 2019.

Bartlein, P. J., et al.: Pollen-based continental climate reconstructions at 6 and 21 ka: A global synthesis, Clim. Dyn., 37, 775-802, doi:10.1007/s00382-010-0904-1, 2011.

Beghin, P., Charbit, S., Kageyama, M., Combourieu-Nebout, N., Hatté, C., Dumas, C., Peterschmitt, J.-Y.: What drives LGM precipitation over the western Mediterranean? A study focused on the Iberian Peninsula and northern Morocco, Clim. Dyn., 46, 2611- 2631, doi:10.1007/s00382-015-2720-0, 2016.

Bengtsson L., Hodges K.I., and Keenlyside N.: Will extratropical storms intensify in a warmer climate? J. Clim. 22: 2276–2301, doi:10.1175/2008JCLI2678.1, 2009.

Born K., Ludwig P., Pinto J.G.: Wind gust estimation for Mid-European winter storms: Towards a probabilistic view. Tellus A, 64, 17471, doi:10.3402/tellusa.v64i0.17471, 2012.

Braconnot, P., Harrison, S. P., Kageyama, M., Bartlein, P. J., Masson-Delmotte, V., Abe-Ouchi, A., Otto-Bliesner, B., and Zhao, Y.: Evaluation of climate models using palaeoclimatic data, Nat. Clim. Change, 2, 417– 424, doi:10.1038/nclimate1456, 2012.

Catto, J.L., Ackerley, D., Booth, J., Champion, A., Colle, B., Pfahl, S., Pinto, J.G., Quinting, J., and Seiler, C.: The Future of Extratropical Cyclones. Curr Clim Change Rep, doi:10.1007/s40641-019-00149-4, 2019.

Catto, J. L., Shaffrey, L. C., and Hodges, K. I.: Can climate models capture the structure of extratropical cyclones?, J. Clim., 23, 1621– 1635. doi:10.1175/2009JCLI3318.1, 2010.

Chang, E.K. M., Lee, S., and Swanson, K.L.: Storm track dynamics. J. Clim.,15, 2163–2183, doi: 10.1175/1520-0442(2002)015<02163:STD>2.0.CO;2, 2002.

Clark, P.U., et al.: The Last Glacial Maximum. Science 325, 710–714. doi:10.1126/science.1172873, 2009.

Cleator, S.F., Harrison, S.P., Nichols, N.K., Prentice, I.C., and Roulstone, I.: A new multi-variable benchmark for Last Glacial Maximum climate simulations, Clim. Past Discuss., doi:10.5194/cp-2019-55, 2019.

CLIMAP Project Members: The last interglacial ocean, Quat. Res., 2, 123–224, doi:10.1016/0033-5894(84)90098-X, 1984.

Dacre, H.F., Hawcroft, M.K., Stringer, M.A., and Hodges, K.I.: An extratropical cyclone database: A tool for illustrating cyclone structure and evolution characteristics, Bull. Amer. Met. Soc., doi: 10.1175/BAMS-D-11-00164.1, 2012.

Donohoe, A., and Battisti, D.S.: Causes of Reduced North Atlantic Storm Activity in a CAM3 Simulation of the Last Glacial Maximum. J. Climate, 22, 4793–4808, doi:10.1175/2009JCLI2776.1, 2009.

Ferrier, B. S., Tao, W.-K., and Simpson, J.: A double-moment multiple-phase four-class bulk ice scheme. Part II: Simulations of convective storms in different large-scale environments and comparisons with other bulk parameterizations, Journal of the atmospheric sciences, 52, 8, 1001-1033, doi: 10.1175/1520-0469(1995)052<1001:ADMMPF>2.0.CO;2, 1995.

Fitzsimmons, K.E., Markovic, S. B., and Hambach, U.: Pleistocene environmental dynamics recorded in the loess of the middle and lower Danube basin, Quaternary Science Reviews, 41, 104–118, doi:10.1016/j.quascirev.2012.03.002, 2012.

Hawcroft, M.K., Shaffrey, L.C., Hodges, K.I., and Dacre, H.F.: How much Northern Hemisphere precipitation is associated with extratropical cyclones?, Geophys. Res. Lett., 39, L24809, doi:10.1029/2012GL053866, 2012.

Hawcroft, M.K., Shaffrey, L.C., Hodges, K.I., and Dacre, H.F.: Can climate models represent the precipitation associated with extratropical cyclones?, Clim. Dyn., 47: 679–695, doi:10.1007/s00382-015-2863-z, 2016.

Harrison, S.P., Bartlein, P.J., Izumi, K., Li, G., Annan, J., Hargreaves, J., Braconnot, P., and Kageyama, M.: Evaluation of CMIP5 palaeo-simulations to improve climate projections, Nat. Clim. Chang., 5, 735-743, doi:10.1038/nclimate2649, 2015.

Harrison, S.P., Bartlein, P. J., and Prentice, I.C.: What have we learnt from palaeoclimate simulations?, J. Quat. Sci., 31, 363–385, doi:10.1002/jqs.2842, 2016.

Hewson, T. D., and Neu U.: Cyclones, windstorms and the IMILAST project, Tellus A, 67, 27128, doi:10.3402/tellusa.v67.27128, 2015.

Hofer, D., Raible, C.C., Dehnert, A., and Kuhlemann, J.: The impact of different glacial boundary conditions on atmospheric dynamics and precipitation in the North Atlantic region, Clim. Past, 8, 935– 949, doi:10.5194/cp-8-935-2012, 2012.

Hoskins B.J., and Hodges K.I.: New perspectives on the Northern Hemisphere winter storm tracks. J. Atmos. Sci. 59: 1041 – 1061, doi:10.1175/1520-0469(2002)059<1041:NPOTNH>2.0.CO;2, 1990.

Hoskins, B.J., and Valdes, P. J.: On the existence of storm tracks, J. Atmos. Sci., 47, 1854– 1864. doi:10.1175/1520-0469(1990)047<1854:OTEOST>2.0.CO;2, 1990.

Iacono, M.J., Delamere, J.S., Mlawer, E.J., Shephard, M.W., Clough, S.A., and Collins W.D.: Radiative forcing by long–lived greenhouse gases: Calculations with the AER radiative transfer models. J. Geophys. Res., 113, D13103. doi:10.1029/2008JD009944, 2008

Ishizuka, M., Mikami, M., Leys, J., Yamada, Y., Heidenreich, S., Shao, Y., and McTainsh, G. H.: Effects of soil moisture and dried raindroplet crust on saltation and dust emission, J. Geophys. Res., 113, D24212, doi:10.1029/2008JD009955, 2008.

Janjić, Z.I.: The Step-Mountain Eta Coordinate Model: Further Developments of the Convection, Viscous Sublayer, and Turbulence Closure Schemes. Mon. Wea. Rev., 122, 927–945, doi:10.1175/1520-0493(1994)122<0927:TSMECM>2.0.CO;2, 1994.

Jungclaus, J. H., Fischer, N., Haak, H., Lohmann, K, Marotzke, J., Matei, D., Mikolajewicz, U., Notz, D., and von Storch, J.-S.: Characteristics of the ocean simulations in the Max Planck Institute Ocean Model (MPIOM) the ocean component of the MPI-Earth system model. J. Adv. Model. Earth Syst., 5, 422–446, doi: 10.1002/jame.20023, 2013.

Kageyama, M., Valdes, P. J., Ramstein, G., Hewitt, C., and Wyputta, U.: Northern Hemisphere storm tracks in present day and Last Glacial Maximum climate simulations: A comparison of the European PMIP models, J. Clim., 12, 742– 760, doi:10.1175/1520-0442(1999)012<0742:NHSTIP>2.0.CO;2, 1999.

Kageyama, M., et al.: The PMIP4 contribution to CMIP6 – Part 4: Scientific objectives and experimental design of the PMIP4-CMIP6 Last Glacial Maximum experiments and PMIP4 sensitivity experiments. Geosci. Model Dev., 10, 4035–4055, doi:10.5194/gmd-10-4035-2017, 2017.

Kageyama, M., et al.: The PMIP4 contribution to CMIP6 – Part 1: Overview and overarching analysis plan. Geosci. Model Dev., 11, 1033–1057, doi: 10.5194/gmd-11-1033-2018, 2018.

Kalnay, E., M. et al.: The NCEP/NCAR 40-Year Reanalysis Project. Bull. Amer. Meteor. Soc., 77, 437–472, doi:10.1175/1520-0477(1996)077<0437:TNYRP>2.0.CO;2, 1996.

Laîné, A., Kageyama, M., Salas-Mélia, D., Voldoire, A., Rivière, G., Ramstein, G., Planton, S., Tyteca, S., and Peterschmitt, J.Y.: Northern Hemisphere storm tracks during the Last Glacial Maximum in the PMIP2 ocean-atmosphere coupled models: Energetic study, seasonal cycle, precipitation, Clim. Dyn., 32, 593-614, doi:10.1007/s00382-008-0391-9, 2009.

Lambeck, K., and Chappell, J.: Sea level change through the last glacial cycle, Science, 292, 679– 686, doi:10.1126/science.1059549, 2001.

Lambeck, K., Yokoyama, Y., and Purcell, A.: Into and out of the Last glacial Maximum sea level change during Oxygen Isotope Stages 3–2, Quat. Sci. Rev., 21, 343– 360, doi:10.1016/S0277-3791(01)00071-3, 2002.

Löfverström, M., Caballero, R., Nilsson, J., and Kleman, J.: Evolution of the large-scale atmospheric circulation in response to changing ice sheets over the last glacial cycle, Clim. Past, 10, 1453-1471, doi:10.5194/cp-10-1453-2014, 2014.

Löfverström, M., Caballero, R., Nilsson, J., and Messori, G.: Stationary wave reflection as a mechanism for zonalising Atlantic winter jet at the LGM, J. Atmos. Sci., 73, 3329– 3342, doi:10.1175/JAS-D-15-0295.1, 2016.

Löfverström, M: A dynamic link between high-intensity precipitation events in southwestern North America and Europe at the Last Glacial Maximum, Earth Planet. Sci. Lett., 534, 116081, doi:10.1016/j.epsl.2020.116081, 2020

Luetscher, M., Boch, R., Sodemann, H., Spötl, C., Cheng, H., Edwards, R.L., Frisia, S., Hof, F., and Muller, W.: North Atlantic storm track changes during the Last Glacial Maximum recorded by Alpine speleothems, Nat. Commun., 6, 6344,doi:10.1038/ncomms7344, 2015.

Ludwig, P., Pinto, J.G., Hoepp, S.A., Fink, A.H., and Gray, S.L.: Secondary cyclogenesis along an occluded front leading to damaging wind gusts: windstorm Kyrill, January 2007. Mon Weather Rev, 143, 1417–1437. doi:10.1175/MWR-D-14-00304.1, 2015.

Ludwig, P., Schaffernicht, E.J., Shao, Y., and Pinto, J.G.: Regional atmospheric circulation over Europe during the Last Glacial Maximum and its links to precipitation, J. Geophys. Res. Atmos., 121, 2130-2145, doi:10.1002/2015JD024444, 2016.

Ludwig, P., Pinto, J.G., Raible, C.C., and Shao,Y.: Impacts of surface boundary conditions on regional climate model simulations of European climate during the Last Glacial Maximum, Geophys. Res. Lett., 44, 5086– 5095, doi:10.1002/2017GL073622, 2017.

Ludwig, P., Shao, Y., Kehl, M., Weniger, G.-C.: The Last Glacial Maximum and Heinrich event I on the Iberian Peninsula: A regional climate modelling study for understanding human settlement patterns. Global and planetary change, 170, 34–47. doi:10.1016/j.gloplacha.2018.08.006, 2018.

Ludwig, P., Gómez-Navarro, J.J., Pinto, J.G., Raible, C.C., Wagner, S. and Zorita, E.: Perspectives of regional paleoclimate modeling. Ann. N.Y. Acad. Sci., 1436: 54-69. doi:10.1111/nyas.13865, 2019.

Maher, B.A., Prospero, J.M., Mackie, D., Gaiero, D., Hesse, P.P., and Balkanski, Y.: Global connections between aeolian dust, climate and ocean biogeochemistry at the present day and at the last glacial maximum, Earth-Science Reviews, 99, 61–97, doi:10.1016/j.earscirev.2009.12.001, 2010.

Merz, N., Raible, C.C., and Woollings, T.: North Atlantic eddy-driven jet in interglacial and glacial winter climates, J. Clim., 28, 3977-3997, doi:10.1175/JCLI-D-14-00525, 2015.

Moreno, A., Svensson, A., Brooks, S.J., Connor, S., Engels, S., Fletcher, W., Genty, D., Heiri, O., Labuhn, I., Perşoiu, A., Peyron, O., Sadori, L., Valero-Garcés, B., Wulf, S., and Zanchetta, G.: A compilation of western European terrestrial records 60-8kaBP: towards an understanding of latitudinal climatic gradients. Quat. Sci. Rev. 106, 167–185. doi:10.1016/j.quascirev.2014.06.030, 2014.

Murray, R.J., and Simmonds, I.: A numerical scheme for tracking cyclone centres from digital data. Part I: Development and operation of the scheme, Aust. Meteorol. Mag., 39, 155– 166, 1991.

Neu, U., et al.: IMILAST: A community effort to intercompare extratropical cyclone detection and tracking algorithms, Bull. Am. Meteorol. Soc., 94, 529– 547. doi:10.1175/BAMS-D-11-00154.1, 2013.

Peltier, W.R., Argus, D.F., and Drummond, R.: Space geodesy constrains ice age terminal deglaciation: The global ICE-6G_C (VM5a) model, J. Geophys. Res. Solid Earth, 119, 450-487, doi:10.1002/2014JB011176, 2015.

Pfahl, S., and Wernli, H.: Quantifying the Relevance of Cyclones for Precipitation Extremes. J. Climate, 25, 6770–6780, doi:10.1175/JCLI-D-11-00705.1, 2012.

Pfahl, S., O'Gorman, P., and Singh, M.S.: Extratropical cyclones in idealized simulations of changed climates, J. Clim., 28, 9373-9392, doi:10.1175/JCLI-D-14-00816.1, 2015.

Pinto. J.G., Ulbrich, U., Leckebusch, G.C., Spangehl, T., Reyers, M., Zacharias, S.: Changes in storm track and cyclone activity in three SRES ensemble experiments with the ECHAM5/MPI-OM1 GCM. Clim Dyn 29, 195–210. doi:10.1007/s00382-007-0230-4, 2007.

Pinto, J.G., Zacharias, S., Fink, A.H., Leckebusch, G.C., and Ulbrich, U.: Factors contributing to the development of extreme North Atlantic cyclones and their relationship with the NAO, Clim. Dyn., 32, 711-737. doi:10.1007/s00382-008-0396-4, 2009.

Prospero, J.M., Ginoux, P., Torres, O., Nicholson, S.E., and Gill, T.E.: Environmental characterization of global sources of atmospheric soil dust identified with the Nimbus 7 Total Ozone Mapping Spectrometer (TOMS) Absorbing Aerosol Product, Rev. Geophys., 40, 1002, doi:10.1029/2000RG000095, 2002.

Raible, C.C., Messmer, M., Lehner, F., Stocker, T.F., Blender, R.: Extratropical cyclone statistics during the last millennium and the 21st century. Clim. Past, 14, 1499-1514, doi: 10.5194/cp-14-1499-2018., 2018.

Ray, N., Adams, J.M.: A GIS-based Vegetation Map of the World at the Last Glacial Maximum (25,000–15,000 BP). Internet Archaeology, 11. doi:10.11141/ia.11.2, 2001.

Riviére, G., Lainé, A., Lapeyre, G., Salas-Mélia, D., and Kageyama, M.: Links between Rossby wave breaking and the North Atlantic Oscillation–Arctic Oscillation in present day and Last Glacial Maximum climate simulations. J Clim, 23, 2987–3008, doi:10.1175/2010JCLI3372.1, 2010.

Rivière, G., Berthou, S., Lapeyre, G., and Kageyama, M.: On the Reduced North Atlantic Storminess during the Last Glacial Period: The Role of Topography in Shaping Synoptic Eddies. J. Climate, 31, 1637–1652, doi:10.1175/JCLI-D-17-0247.1, 2018

Rudeva, I., Gulev S.K.: Composite Analysis of North Atlantic Extratropical Cyclones in NCEP–NCAR Reanalysis Data. Mon Wea Rev, 139, 1419–1446, doi:10.1175/2010MWR3294.1, 2011.

Schaffernicht, E.J., Ludwig, P., and Shao, Y.: Linkage between Dust Cycle and Loess of the Last Glacial Maximum in Europe. Atmos. Chem. Phys. Discuss., doi:10.5194/acp-2019-693, 2019.

Schulz, J.-P.: Revision of the turbulent gust diagnostics in the COSMO model. COSMO Newsletter 8, 17-22. Online at: www.cosmo-model.org, 2008.

Schulz, J.-P., and Heise, E.: A new scheme for diagnosing near-surface convective gusts. COSMO Newsletter 3, 221-225.Online at: www.cosmo-model.org, 2003.

Sinclair, V. A., Rantanen, M., Haapanala, P., Räisänen, J., and Järvinen, H.: The characteristics and structure of extra-tropical cyclones in a warmer climate, Weather Clim. Dynam. Discuss., doi:10.5194/wcd-2019-2, 2019.

Skamarock, W.C., Klemp, J. B., Dudhia, J., Gill, D.O., Barker, D.M., Duda, M.G., Huang, X.-Y., Wang, W., and Powers, J. G.: A description of the advanced research WRF version 3, NCAR Tech. Note NCAR/TN-475+STR, 113 pp., doi:10.5065/D68S4MVH, 2008.

Shao, Y., Anhäuser, A., Ludwig, P., Schlüter, P., and Williams, E.: Statistical reconstruction of global vegetation for the last glacial maximum, Global Planet Change, 168, 67-77, doi:10.1016/j.gloplacha.2018.06.002, 2018.

Shao, Y., Wyrwoll, K.-H., Chappell, A., Huang, J., Lin, Z., McTainsh, G.H., Mikami, M., Tanaka, T.Y., Wang, X., and Yoon, S.: Dust cycle: An emerging core theme in Earth system science, Aeol. Res., 2, 181-204, 2011.

Stevens, B., et al.: Atmospheric component of the MPI-M Earth system model: ECHAM6, J. Adv. Model. Earth Syst., 5, 146-172, doi:10.1002/jame.20015, 2013.

Tarasov, L., and Peltier, W. R.:Greenland glacial history and local geodynamic consequences, Geophys. J. Int., 150, 198-229, doi:10.1046/j.1365-246X.2002.01702.x, 2002.

Tarasov, L., and Peltier, W.R.: Greenland glacial history, borehole constraints, and Eemian extent, J. Geophys. Res., 108, 2143, doi:10.1029/2001JB001731, 2003.

Tewari, M., Chen, F., Wang, W., Dudhia, J., LeMone, M.A., Mitchell, K., Ek, M., Gayno, G., Wegiel J., and Cuenca, R.H.: Implementation and verification of the unified NOAH land surface model in the WRF model, 20th conference on weather analysis and forecasting/16th conference on numerical weather prediction, pp. 11–15, 2004

Ugan, A., and Byers, D.: Geographic and temporal trends in proboscidean and human radiocarbon histories during the late Pleistocene, Quaternary Science Reviews, 26, 3058–3080, doi:10.1016/j.quascirev.2007.06.024, 2007.

Újvári, G., Stevens, T., Molnár, M., Demény, A., Lambert, F., Varga, G., Jull, AJT., Páll-Gergely, B., Buylaert, J.P., and Kovács, J.: Coupled European and Greenland last glacial dust activity driven by North Atlantic climate. Proc Natl Acad Sci USA, 114, E10632-E10638, doi:10.1073/pnas.1712651114, 2017

Ulbrich, U., Leckebusch, G. C., and Pinto, J. G.: Extra-tropical cyclones in the present and future climate: A review, Theor. Appl. Climatol., 96, 117-131. doi:10.1007/s00704-008-0083-8, 2009.

Wang, N., Jiang, D., and Lang, X.: Northern Westerlies during the Last Glacial Maximum: results from CMIP5 simulations. J. Clim. 31, 1135-1153. Doi: 10.1175/JCLI-D-17-0314.1, 2018.

Wernli H., Dirren S., Liniger M.A., and Zillig M.: Dynamical aspects of the life cycle of the winter storm 'Lothar' (24–26 December 1999). Q. J. R. Meteorol. Soc., 128, 405– 429. doi:10.1256/003590002321042036, 2002.

Zhang, C., Wang, Y., and Hamilton, K.: Improved Representation of Boundary Layer Clouds over the Southeast Pacific in ARW-WRF Using a Modified Tiedtke Cumulus Parameterization Scheme. Mon. Wea. Rev., 139, 3489–3513, doi:10.1175/MWR-D-10-05091.1, 2011.

Tables

Table 1. Boundary conditions adapted in the WRF simulations for PI and LGM based on the PMIP3 protocol.

	CO_2	N_2O	CH_4	Eccentricity	Obliquity	Angular Precession
PI	280 ppm	270 ppb	760 ppb	0.01672	23.446 °	102.04
LGM	185 ppm	200 ppb	350 ppb	0.01899	22.949 °	114.42

Table 2. Physical parametrization schemes used in the regional model simulations (same parametrizations used for 50 km and 12.5 km domain).

	microphysics	cumulus scheme	PBL-scheme	Radiation scheme	surface
WRF-namelist option	**95** (Eta (Ferrier))	**6** (Tiedke)	**2** (Mellor–Yamada–Janjic)	SW/LW: **4** (RRTMG)	**2** (Noah–LSM)
Reference	Ferrier et al. (1995)	Zhang et al. (2011)	Janjic (1994)	Iacono et al. (2008)	Tewari et al. (2004)

Table 3. Overview of time and location of maximum intensity (defined by the maximum of the Laplacian of mslp) of the TOP 30 MPI-ESM-P cyclones for PI and LGM conditions inside the box (Figure 1).

	PI					LGM				
	Date	Time	Lapl P	°Lat	°Lon	Date	Time	Lapl P	°Lat	°Lon
1	2993010	18	3.162	51.54	342.98	1936021	00	3.535	52.33	338.93
2	2996010	12	3.158	51.96	343.35	1931101	18	3.430	47.35	335.87
3	2990112	18	2.858	44.31	340.09	1936112	00	3.220	46.53	341.67
4	2994110	18	2.811	41.67	339.00	1942102	06	3.202	52.34	345.53
5	2983031	06	2.786	45.87	335.95	1922011	06	3.067	46.62	337.56
6	2998013	00	2.734	49.97	336.31	1940022	12	2.965	50.20	348.23
7	2994111	06	2.628	49.90	343.87	1941111	06	2.962	49.70	343.95
8	2980011	18	2.615	47.33	347.16	1932111	00	2.917	52.11	346.19
9	2998022	18	2.572	49.45	335.94	1927112	06	2.911	43.70	337.33
10	2999102	12	2.551	50.82	345.56	1921122	06	2.894	45.19	345.36
11	2983123	06	2.541	41.97	336.09	1925111	18	2.850	46.88	348.18
12	2985112	12	2.528	48.60	349.10	1944012	00	2.823	43.52	335.73
13	2999020	18	2.512	43.76	344.89	1940032	18	2.812	49.81	335.18
14	2994020	12	2.511	46.31	345.74	1942011	00	2.746	52.13	337.36
15	2989122	00	2.493	51.81	342.91	1937102	00	2.728	45.43	348.59
16	2979022	00	2.491	50.35	344.83	1923032	18	2.725	50.70	349.34
17	3003120	06	2.489	42.45	344.77	1940110	18	2.688	51.82	346.50
18	3001010	18	2.473	48.50	339.35	1922010	06	2.679	42.31	342.38
19	2985011	18	2.471	43.52	338.38	1923020	12	2.678	48.73	342.70
20	2987010	12	2.466	47.53	345.43	1935010	18	2.663	51.29	339.74
21	2996112	00	2.457	46.23	337.72	1935121	00	2.635	52.12	342.00
22	3000122	06	2.299	47.43	345.84	1924022	00	2.613	50.39	344.81
23	2990022	18	2.298	51.33	348.96	1933110	06	2611	51.09	341.01
24	2981121	06	2.272	47.65	345.85	1938100	12	2.590	51.91	336.29
25	2991011	00	2.263	49.51	338.82	1943021	06	2.584	48.11	348.10
26	2979112	12	2.252	45.25	349.74	1932021	06	2.507	49.92	345.95
27	3004011	06	2.246	44.70	340.05	1927011	06	2.497	47.66	341.06
28	2997021	18	2.200	48.06	343.77	1937120	00	2.481	43.06	336.95
29	3000032	00	2.167	50.88	341.08	1923020	00	2.478	50.41	347.84
30	3003103	18	2.147	46.78	347.93	1923022	12	2.448	42.46	345.65
	Mean		2.52	47.51	342.72			2.80	48.53	342.53
	Median		2.49	47.59	343.56			2.73	49.76	343.54

530

Figures

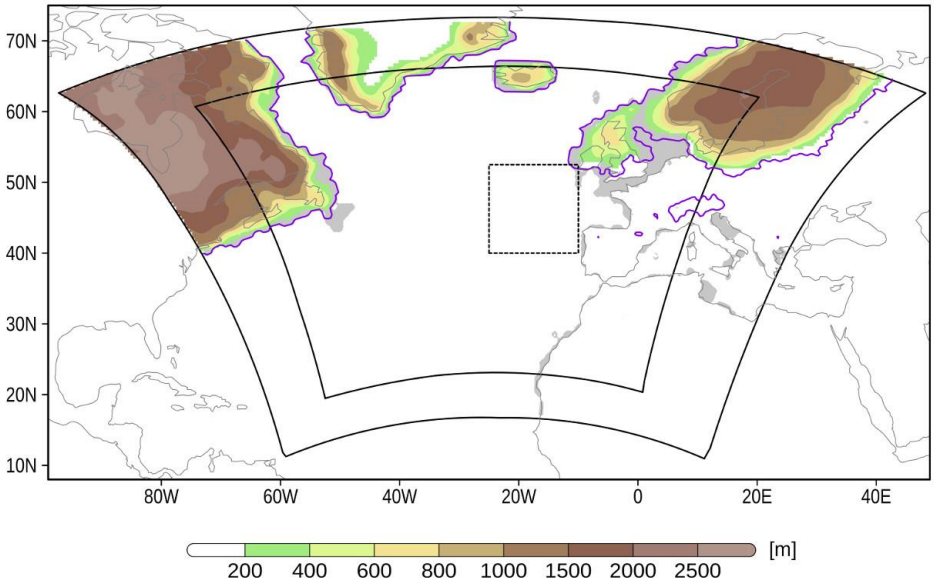

Figure 1. WRF model domains (outer solid box: 50 km grid spacing; inner solid box: 12.5 km grid spacing), ice sheet heights [m] (coloured) and extents (purple line), land sea mask (additional land areas grey) as obtained from PMIP3; target area for cyclone detection marked by dotted box.

535

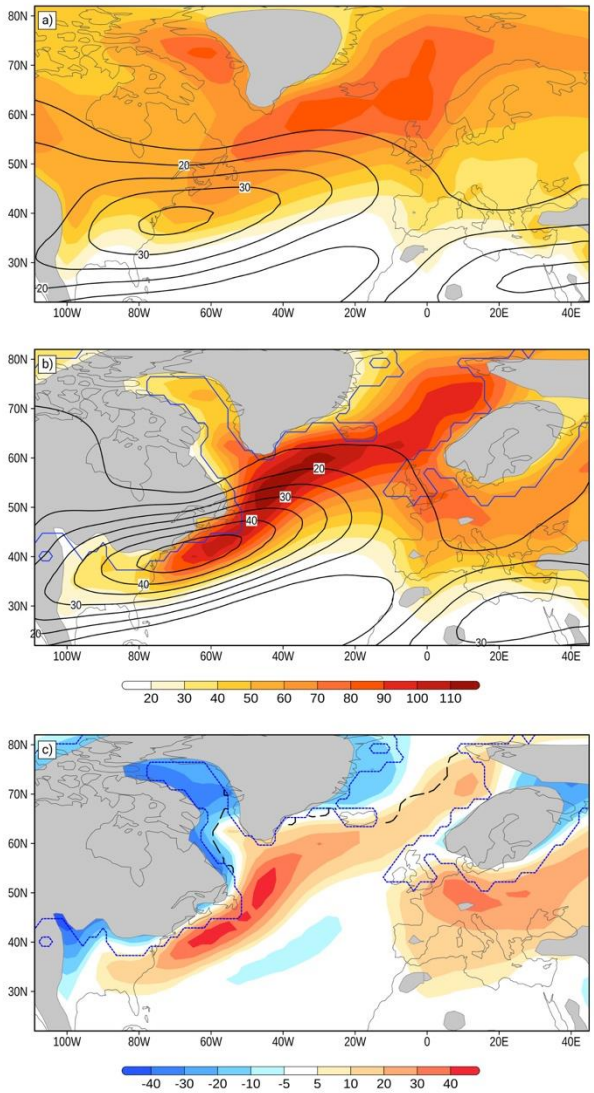

Figure 2. Cyclone track density [cyclone days per extended winter per (deg.lat.)^2] (coloured) and 300 hPa wind speed [m s^{-1}] (contours) based on MPI-ESM-P data for (a) PI, (b) LGM and (c) difference between LGM and PI. Areas with topography higher 1000 m shaded grey, ice sheet margins (b and c) denoted by thin stippled line, long dashed black line in (c) denotes margin of 40% annual sea ice cover.

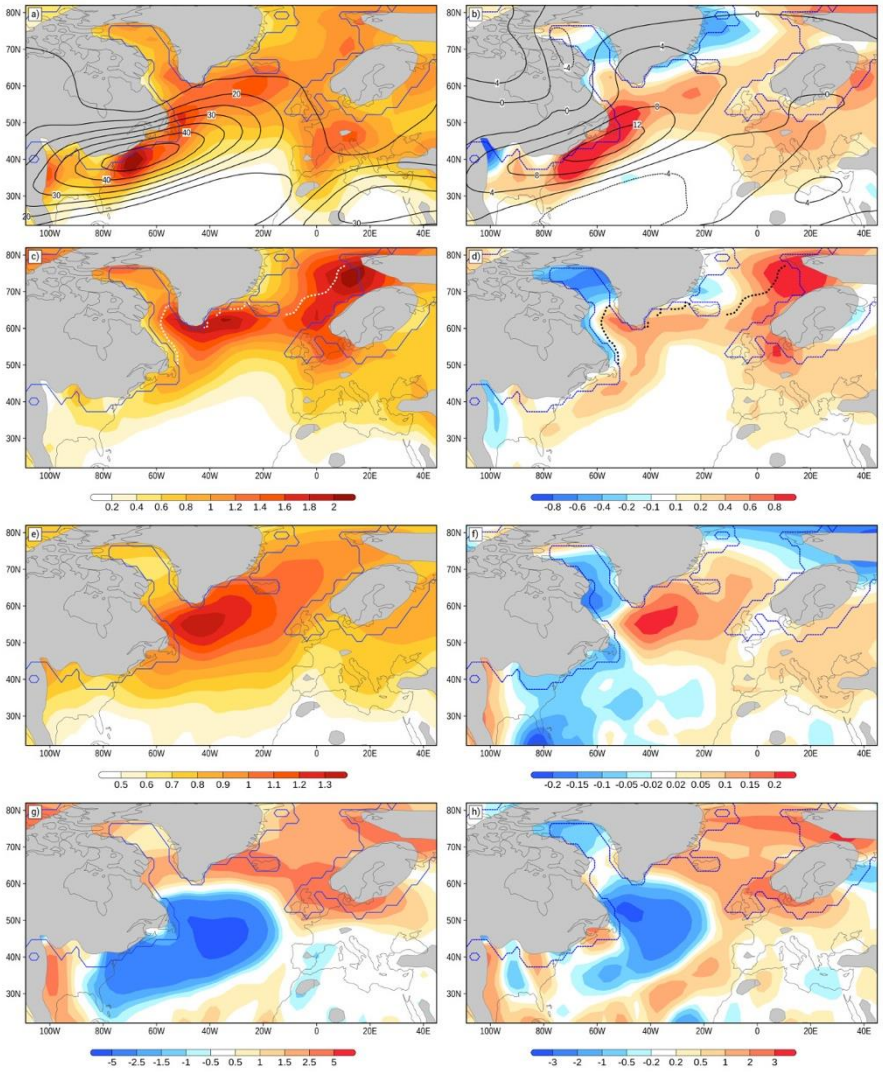

Figure 3. Statistical measures obtained from cyclone tracking algorithm for LGM cyclones (left column) and difference to PI cyclones (right column) for (a), (b) cyclogenesis [events per extended winter per (deg.lat.)^2] (coloured) and wind speed at 300hPa [m s^{-1}] (contours), (c),(d) cyclolysis [events per extended winter per (deg.lat.)^2]; (e), (f) mean Δ MSLP [Laplacian of pressure per extended winter per (deg.lat.)^2] and (g), (h) deepening rates [hPa h^{-1}]. Areas with topography higher 1000 m shaded grey, ice sheet extents marked by the blue line. Sea ice margin (>40% annual cover) in (c) and (d) indicated by bold dashed lines.

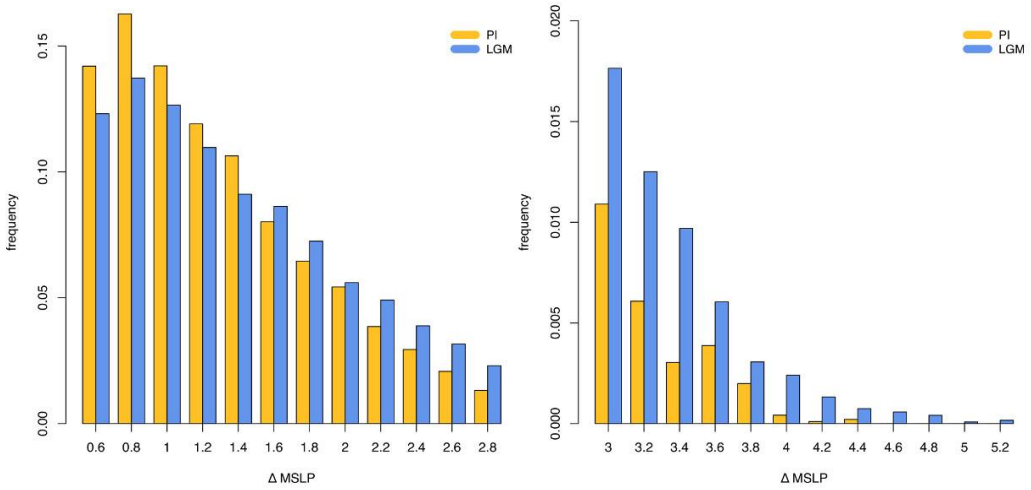

Figure 4. Histogram of cyclone intensity (Laplacian (Δ) MSLP) over the North Atlantic (70°W – 0° and 35°N – 70°N). For intense cyclones (ΔP ≥ 3), the y-axis is adjusted (right panel).

550

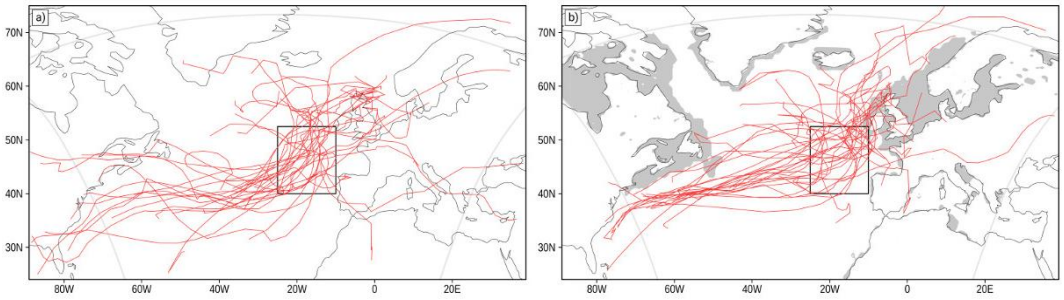

Figure 5. Cyclone tracks of TOP 30 (a) PI and (b) LGM cyclones (MPI-ESM). Black box is region where cyclones need to have maximum intensity to be considered in the composite analysis.

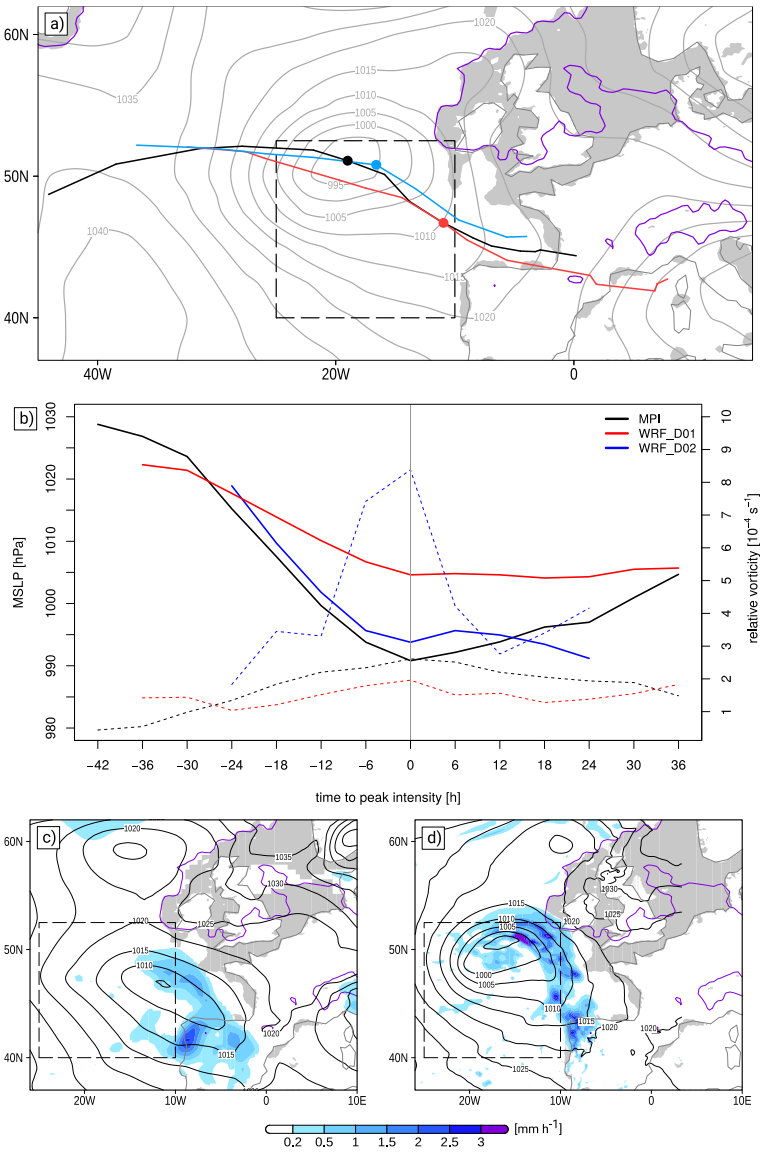

555

Figure 6. Comparison of (a) cyclone tracks for MPI-ESM (black), WRF 50km (red) and WRF 12.5 km (blue) (coloured dots mark the location of peak intensity, black dotted box shows target area) and MSLP [hPa] for MPI-ESM at peak intensity, (b) timeseries of cyclone core pressure and relative vorticity for MPI-ESM, WRF 50km and WRF 12.5 km for LGM cyclone #24. Simulated precipitation rate [mm h^{-1}] (shaded) and MSLP [hPa] (lines) at peak intensity for (c) WRF 50km and (d) WRF
560 12.5km.

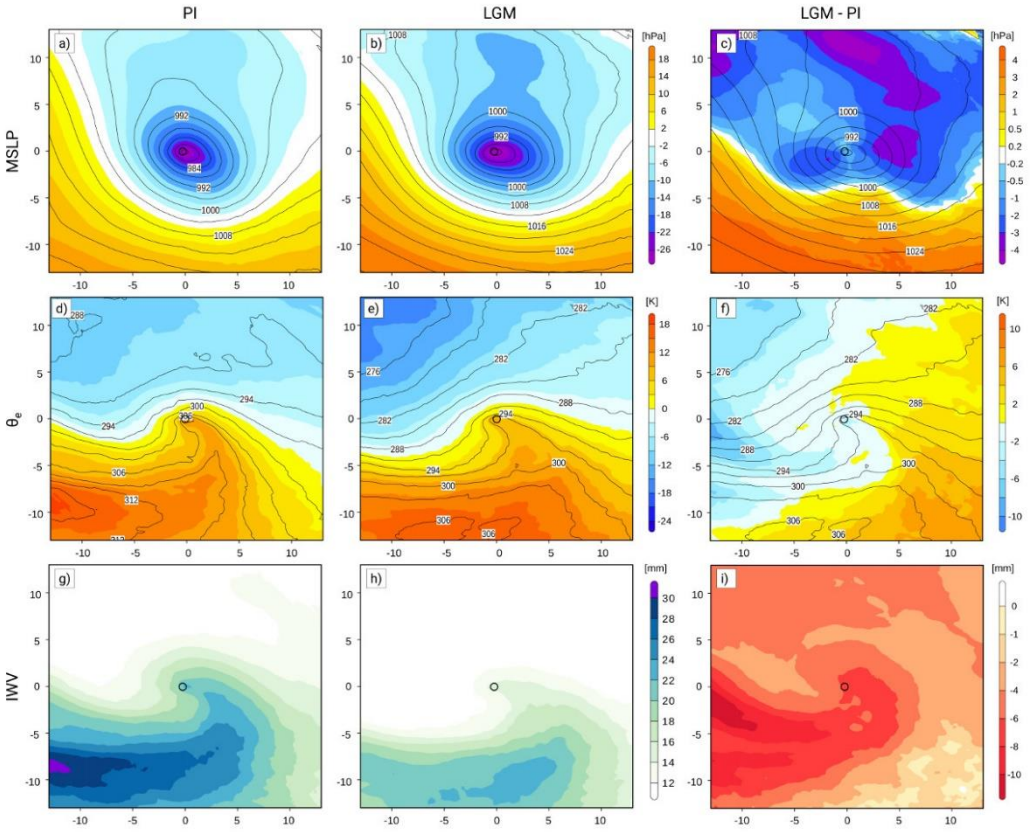

Figure 7. Composites of (a - c) mean sea level pressure, (d - f) ThetaE, and (g - i) vertical integrated water vapour (IWV) for PI, LGM and difference LGM – PI at peak intensity as defined by the maximum of the Laplacian of MSLP. (a, b) absolute MSLP values (lines, [hPa]), anomalies [hPa] from mean over displayed area (coloured); (c) absolute MSLP values (lines, [hPa]) from LGM, differences of the anomalies between LGM – PI in colours; (d, e) absolute ThetaE values (lines, [K]) and anomalies [K] from mean over displayed area (coloured); (f) absolute ThetaE values (lines, [K]) from LGM, differences of the anomalies between LGM – PI in colours; (g, h) absolute IWV values [mm], (i) difference [mm] LGM – PI.

570

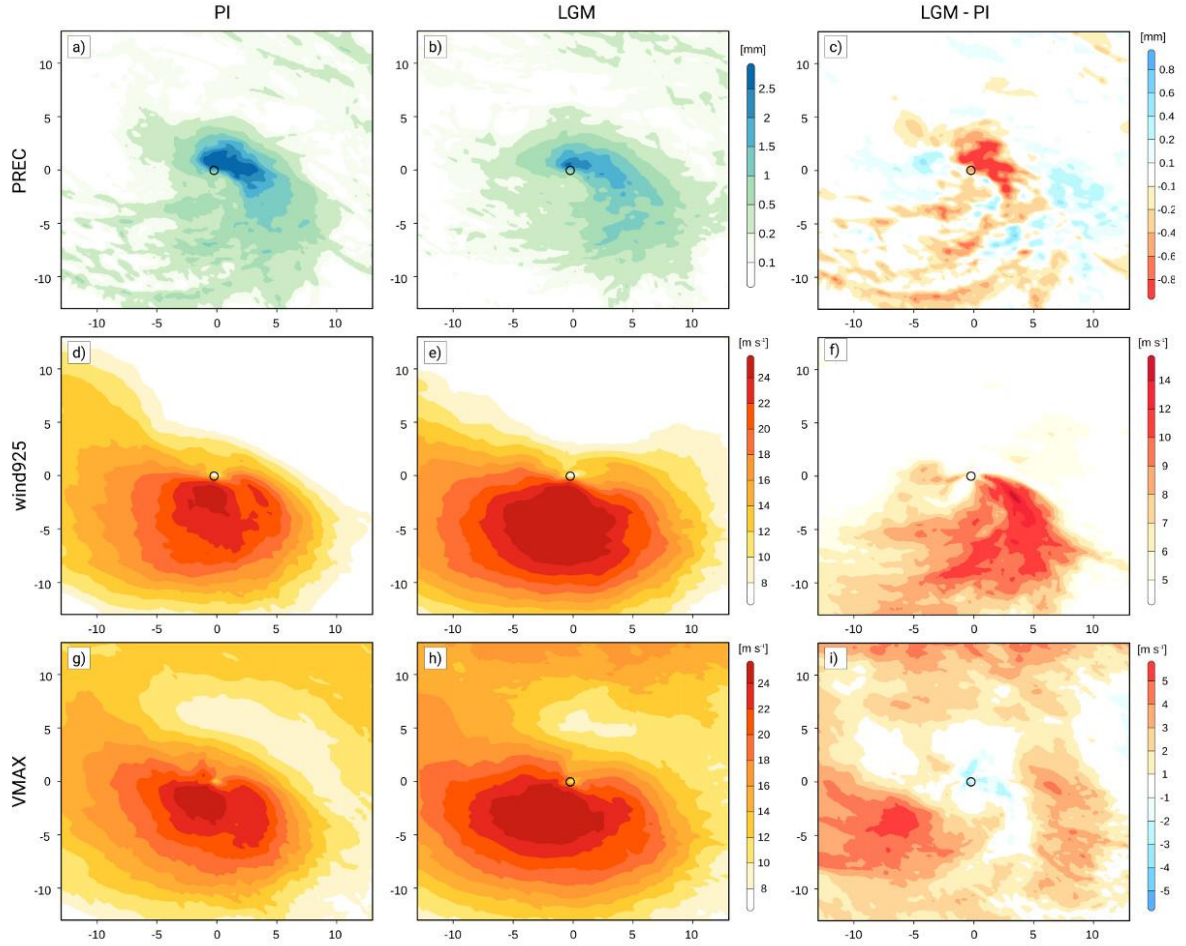

Figure 8. As Figure 7 but for hourly precipitation [mm] (a) PI, (b) LGM, (c) LGM – PI, (d - f) wind speed in 925 hPa [m s^{-1}] and (g - i) maximum near surface wind gust [m s^{-1}] at peak intensity.